University of New Orleans

ScholarWorks@UNO

Physics Faculty Publications   Department of Physics

Novel electronic and magnetic properties of ultrathin chromium oxide films grown on Pt(111)

P S. Robbert
University of New Orleans

H Geisler

C A. Ventrice Jr

J van Ek

S Chaturvedi

See next page for additional authors

Recommended Citation

Authors

P S. Robbert, H Geisler, C A. Ventrice Jr, J van Ek, S Chaturvedi, J A. Rodriguez, M Kuhn, and U Diebold

Novel electronic and magnetic properties of ultrathin chromium oxide films grown on Pt(111)

P. S. Robbert, H. Geisler, and C. A. Ventrice, Jr.[a]
Department of Physics, University of New Orleans, New Orleans, Louisiana 70148

J. van Ek[b]
Seagate Technology, Bloomington, Minnesota 55435

S. Chaturvedi and J. A. Rodriguez[c]
Department of Chemistry, Brookhaven National Laboratory, Upton, New York 11973

M. Kuhn[d] and U. Diebold[e]
Department of Physics, Tulane University, New Orleans, Louisiana 70118

The growth of epitaxial metal–oxide films on lattice-mismatched metal substrates often results in the formation of unique overlayer structures. In particular, epitaxial chromium oxide films grown on Pt(111) exhibit a $p(2 \times 2)$ symmetry through the first two monolayers of growth which is followed by a $(\sqrt{3} \times \sqrt{3})R30°$ phase that is attributed to the growth of a $Cr_2O_3(0001)$ overlayer. Ultraviolet photoelectron spectroscopy measurements have been performed on the $CrO_x/Pt(111)$ system. The electronic structures of CrO_2, Cr_2O_3, and Cr_3O_4 were calculated using the linear muffin-tin orbital method in the atomic sphere approximation. Comparison of the photoemission valence band spectra with the calculated density of states indicates that the CrO_x initially grows in a cubic spinel Cr_3O_4 structure. Beyond ~ 0.2 monolayers, the metallic behavior of the CrO_x overlayer begins a transformation to an insulating state. The measured valence emission for the $p(2 \times 2)$ phase beyond ~ 0.2 monolayers is more consistent with either a γ-$Cr_2O_3(111)$ overlayer or possibly a reconstructed $Cr_2O_3(0001)$ overlayer. © *1998 American Vacuum Society.*
[S0734-2101(98)03503-9]

I. INTRODUCTION

In recent years, the study of the growth of epitaxial metal–oxide/metal interfaces has become a topic of great interest within the surface science community. Besides the advantage of eliminating sample charging problems while performing electron or ion spectroscopies on insulating surfaces, this technique of growing metal oxides also opens up a whole new class of materials that can be studied. For instance, the interaction between the substrate and the metal–oxide overlayer can often result in new structures that are not thermodynamically stable in their bulk forms. One example of this is iron oxide growth on Pt(111) where a well-ordered FeO(111) overlayer, which is not a stable bulk phase of iron oxide at room temperature, is observed during the first monolayer (ML) of growth.[1,2] For NaCl structured metal oxides, stable, polar, surface terminations are not observed for bulk single crystals without the introduction of surface impurities. However, a $p(2 \times 2)$ reconstructed polar NiO(111) surface can be formed during the first few monolayers of growth on the Au(111) substrate.[3,4] In addition, for several metal oxides high-quality bulk single crystals are not readily available, yet well-ordered ultrathin films can often be grown on various single-crystal metal substrates.[5]

Chromium oxide ultrathin films are of interest due to the wide variety of their technological applications. The most stable phase of chromium oxide is the corundum structured Cr_2O_3. This form of the oxide is an important industrial catalyst which is often used in polymerization reactions. In addition, the passivating of stainless steel is accomplished by the formation of a Cr_2O_3/NiO surface complex. Another stable form of chromium oxide is CrO_2. It is a conducting ferromagnet and is used in magnetic recording media because of its resistance to corrosion and its high coercivity. Above 280 °C, CrO_2 decomposes into Cr_2O_3.[6] The stable form of chromium oxide above ~ 1600 °C is a tetragonally distorted Cr_3O_4 spinel phase.[7] The formation of a cubic spinel γ-Cr_2O_3 has also been reported under certain thin-film growth conditions.[8] Well-ordered single crystals of any of the phases of chromium oxide are not readily available.

The growth of chromium oxide on the Pt(111) surface has been studied previously by Zhang *et al.* using low energy electron diffraction (LEED), scanning tunneling microscopy (STM), x-ray photoelectron spectroscopy (XPS), and ion scattering spectroscopy (ISS).[9] The LEED results indicate the formation of a film with a $p(2 \times 2)$ pattern with respect to the Pt(111) substrate during the initial 2 ML of growth which is followed by the formation of $(\sqrt{3} \times \sqrt{3})R30°$ pattern at higher coverages. The growth morphology observed with

STM shows that the CrO_x initially nucleates at step edges and then propagates out in a step flow growth mode with a 2 ML film height. Monitoring of the Cr $2p$ core emission with XPS has revealed a broadening of the emission in the $p(2 \times 2)$ regime with respect to the $(\sqrt{3} \times \sqrt{3})R30°$ regime. In addition, no intermixing of Pt in the CrO_x film is observed with ISS. The $(\sqrt{3} \times \sqrt{3})R30°$ epitaxial phase has been attributed to a $Cr_2O_3(0001)$ overlayer since this would produce a $(\sqrt{3} \times \sqrt{3})R30°$ LEED pattern with respect to the Pt(111) substrate. The results for the $p(2 \times 2)$ phase give evidence for the formation of a Cr_3O_4 cubic spinel phase. Along the [111] direction, the spinel structure consists of close-packed oxygen layers in an $ABC-ABC$ stacking pattern. Between each oxygen layer is a chromium layer with either only octahedrally coordinated or both tetrahedrally and octahedrally coordinated Cr ions. Therefore, broadening of the Cr $2p$ emission is expected since there are two distinct Cr coordinations, and a 2 ML growth mode is expected since the repeat unit consists of two close-packed oxygen layers with their respective Cr intralayers.

In this article, the results of synchrotron-based ultraviolet photoelectron spectroscopy (UPS) measurements of the valence structure of chromium oxide films grown on a Pt(111) substrate are presented. Calculations of the bulk electronic structures of CrO_2, Cr_2O_3, and Cr_3O_4 using the linear muffin-tin orbital method in the atomic sphere approximation (LMTO-ASA) have also been performed. These calculations predict metallic behavior for both CrO_2 and Cr_3O_4. In addition, CrO_2 is predicted to have the unique property of being a perfect half-metallic ferromagnet, and the Cr_3O_4 calculations show an almost perfect half-metallic ferrimagnetic behavior. For Cr_2O_3, an insulating antiferromagnetic behavior is predicted. The results of the electronic structure calculations are compared with the UPS measurements. Within the $(\sqrt{3} \times \sqrt{3})R30°$ chromium oxide growth regime, there is good agreement between the valence structure measured with UPS and the calculated electronic structure of Cr_2O_3. At coverages less than ~ 0.2 ML, a metallic behavior for the overlayer is observed, and the electronic structure calculated for Cr_3O_4 closely mimics the UPS measurements. The measured valence structure of the $p(2 \times 2)$ overlayer beyond ~ 0.2 ML shows a transition to an insulating behavior similar to the $(\sqrt{3} \times \sqrt{3})R30°$ regime. This valence structure is indicative of either a γ-$Cr_2O_3(111)$ or a reconstructed $Cr_2O_3(0001)$ overlayer.

The reactivity of the CrO_x films towards H_2S adsorption has also been examined with UPS. Since the primary emphasis of this article is the electronic and magnetic structure of the CrO_x films, the chemical properties of these films have been published in a separate article.[10]

II. EXPERIMENTAL PROCEDURE

The UPS measurements were performed at the National Synchrotron Light Source (NSLS) at Brookhaven National Laboratory. The primary measurements for this study were carried out at beamline U4A which is equipped with a 6 m toroidal grating monochrometer (TGM). The ultrahigh vacuum (UHV) end station incorporates a hemispherical analyzer for detection of the photoelectrons, a LEED apparatus, and a sputter gun for cleaning the sample. The base pressure of the chamber was 4×10^{-10} Torr. Cleaning of the Pt(111) crystal was achieved by sputtering with Ne ions at 1000 eV for ~ 45 min, followed by annealing the sample to 1000 °C for 5 min. The sample was heated by electron bombardment from a Ta filament. The $x-y$ sample manipulator which was used for the measurements at U4A could not bring the sample within the focal point of the fixed position LEED spectrometer which made determining overlayer structures difficult. Therefore, to confirm the transition from the $p(2 \times 2)$ to the $(\sqrt{3} \times \sqrt{3})R30°$ regime, measurements were also made at U7B which had a movable LEED spectrometer. The comparison of the coverages in each system was achieved by measuring the relative heights of the Cr $2p$ and Pt $4f$ core emissions. The U7B beamline is equipped with a plane grating monochrometer (PGM). The end station incorporates similar instrumentation as U4A, except the base pressure was only 8×10^{-10} Torr, and the heating of the sample was achieved by resistive heating of two 0.25 mm diameter tungsten wires that were spot welded to the back of Pt(111) crystal. The maximum sample temperature achieved using resistive heating was ~ 700 °C. Since the system resolution at U4A is much higher than that at U7B (~ 100 and ~ 500 meV, respectively) over the energy range of interest in this study, only UPS spectra from the U4A run are presented in this article.

Chromium was deposited in both systems using a Cr pellet which was enclosed in a resistively heated tungsten wire basket. The evaporator was equipped with a Ta thermal shield and a shutter to control deposition times. The CrO_x films were grown by backfilling the chamber with O_2 to $p = 2 \times 10^{-6}$ Torr and evaporating Cr at a rate of ~ 0.2 ML/min while maintaining the Pt(111) crystal at ~ 300 °C. As mentioned previously, Zhang *et al.*[9] have determined that the conversion of the LEED from a $p(2 \times 2)$ to a $(\sqrt{3} \times \sqrt{3})R30°$ pattern occurs at 2 ML of CrO_x coverage. This was determined from coverage measurements with a quartz crystal microbalance (QCM) and ISS results. Since neither chamber at the NSLS had a QCM or ISS capabilities, our CrO_x coverages are based on the conversion of the LEED image from the $p(2 \times 2)$ to a $(\sqrt{3} \times \sqrt{3})R30°$ pattern and are estimated to be accurate within $\pm 50\%$.

III. METHODOLOGY OF BULK BAND STRUCTURE CALCULATIONS

The electronic structure calculations were performed using the LMTO-ASA method.[11] Exchange and correlation effects are treated within the local spin-density approximation (LSDA) of density functional theory (DFT).[12] Self-consistent solutions to the Kohn–Sham equations are obtained for all electrons in the system using the exchange-correlation potential as parameterized by von Barth and Hedin.[13] The core-electron states are solutions of the single-particle Dirac equation. Scalar relativistic terms are included in the Hamiltonian for the valence and conduction bands. The LMTO basis set
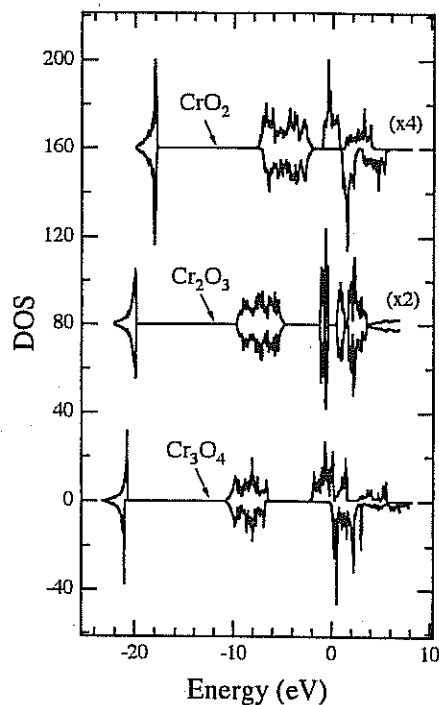
FIG. 1. Calculated spin-resolved density of states for CrO_2, Cr_2O_3, and Cr_3O_4. The majority/minority spin channel is plotted as a positive/negative density of states value.

included $4s$, $4p$, and $3d$-type functions for Cr, and $2s$ and $2p$-type functions for O. Pivotal energies on each site were chosen at the center of gravity of the occupied partial density of states. For CrO_2 empty spheres were introduced in order to improve the description of the interstitial region. Positions of the empty spheres and the sphere radii for all sites were taken from Ref. 14. Atomic sphere radii were taken to be equal for all atoms in Cr_2O_3 and Cr_3O_4, and no empty spheres were employed. A sufficient number of k points was used to sample the irreducible wedges of the Brillouin zones of the three crystals.

The calculations for the rutile-structured CrO_2 and the corundum-structured Cr_2O_3 were performed using the experimentally determined lattice parameters.[8] We know of no previously published experimental data for a bulk-phase, cubic, spinel structured Cr_3O_4. In comparison to the related iron oxide phases, it is noted that there is only a 2% difference in the O–O spacing of α-Fe_2O_3 and Fe_3O_4. Therefore, a lattice parameter of $a_0 = 8.09$ Å, which corresponds to the same O–O nearest neighbor spacing as Cr_2O_3 ($d_{O-O} = 2.86$ Å), was used to calculate electronic structure of the cubic, spinel structured Cr_3O_4. This assumption results in a mismatch of 3% between the surface nets of $Cr_3O_4(111)$ and a $p(2 \times 2)$ Pt(111) which is consistent with the previous LEED results.[9]

IV. RESULTS

A. Spin-resolved electronic structure calculations

The calculated density of states (DOS) for CrO_2, Cr_2O_3, and Cr_3O_4 is shown in Fig. 1. For CrO_2, the majority spin

states cross the Fermi level while the minority spin channel is insulating. Hence, CrO_2 is a half-metallic ferromagnet which is in agreement with the theoretical results of Refs. 14 and 15. As a result of this behavior, the perfect bulk value of the magnetic moment per formula unit is integer $2\mu_B$, where μ_B is the Bohr magneton. Spin-orbit coupling has very little effect on the half-metallic ferromagnetic character of the DOS, as judged from the calculated moment per formula unit of $1.9992\ \mu_B$. The majority and minority Cr $3d$ bands are exchange split by about 2 eV.

The calculated DOS of Cr_2O_3 is shown in Fig. 1. This oxide is an antiferromagnetic insulator. With values of plus and minus 2.8 μ_B, the moments on the Cr atoms in Cr_2O_3 are larger than those in CrO_2. The Cr $3d$ valence band is only ~1 eV wide and is separated from the conduction band by an energy gap of 0.9 eV. Since the experimentally determined band gap of Cr_2O_3 is 3.2 eV,[16,17] these calculations significantly underestimate the magnitude of the band gap which is typical for DFT calculations. The energy separation between the O $2s$ and O $2p$ bands is the same as in CrO_2, but both bands are shifted by ~2 eV to higher binding energy. In addition, the O $2p$ band of Cr_2O_3 is ~5 eV wide which is ~0.5 eV narrower than that for CrO_2.

The calculated DOS for a hypothetical Cr_3O_4 having the spinel structure of its iron oxide analog Fe_3O_4 is shown in Fig. 1. The width of the O $2p$ band is ~4 eV which is narrower than that for either CrO_2 or Cr_2O_3. In addition, both the O $2p$ and O $2s$ bands have shifted ~1.5 eV higher in binding energy than the Cr_2O_3 oxygen bands. The width of the $3d$ band is close to that of the CrO_2 band, and the system is very close to being a half-metallic ferrimagnet. Moments on the two inequivalent Cr atoms are approximately ~1.7 μ_B and 3.2 μ_B, respectively. The ferrimagnetic ordering in Cr_3O_4 is similar to that found in Fe_3O_4 from LSDA calculations.

Since the photoemission measurements reported in this article are not spin resolved, a compilation of the calculated total density of occupied states (sum of minority and majority DOS multiplied by the Fermi function) is shown in Fig. 2 for comparison with the photoemission measurements. There are several differences which are observed in the calculated electronic structures of CrO_2, Cr_2O_3, and Cr_3O_4. As described in the previous section, both CrO_2 and Cr_3O_4 are predicted to be metallic, and there is a successive shift to higher binding energies for the O $2p$ band from CrO_2 to Cr_3O_4. In addition, the relative height of the Cr $3d$ DOS to that of O $2p$ is approximately unity for CrO_2 and Cr_3O_4; whereas, the height of the Cr $3p$ DOS is approximately twice that of O $2p$ for Cr_2O_3.

B. Ultraviolet photoelectron spectroscopy measurements

A series of UPS spectra for CrO_x coverages up to ~4 ML is shown in Fig. 3. At a coverage of 4 ML, no emission features from the Pt(111) substrate are observed; whereas, a superposition of Pt(111) and CrO_x features are observed for
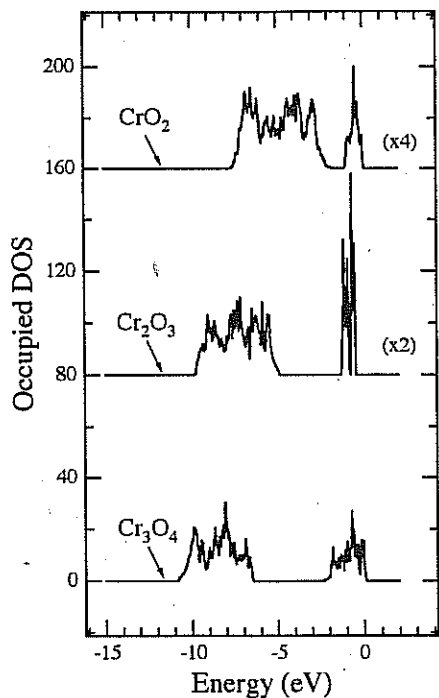
FIG. 2. Calculated total density of occupied states for the valence region of CrO_2, Cr_2O_3, and Cr_3O_4.

the three lower coverages. Spectra from both the clean Pt(111) surface and the surface dosed with 50 L of O_2 are also shown in this series. Slight changes in the valence emission are observed after oxygen dosing which indicates that
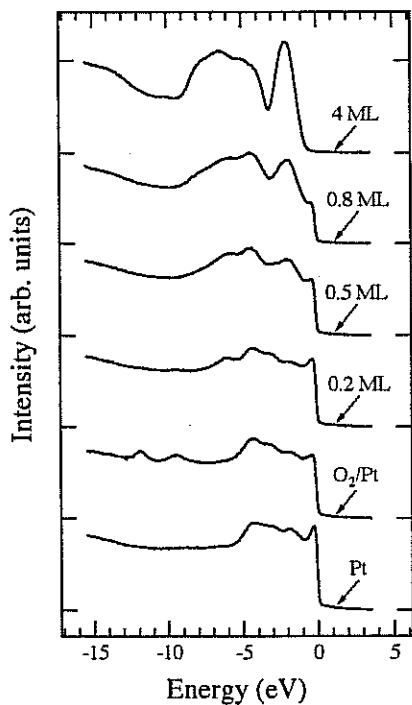

FIG. 3. Measured UPS spectra for CrO_x/Pt(111) coverages up to ~4 ML. The O_2/Pt(111) spectrum corresponds to the dosing of 50 L of oxygen on the clean Pt surface without dosing Cr. All spectra were taken with p-polarized light at an angle of incidence of $\alpha = 45°$, a photon energy of 50 eV, and normal emission.

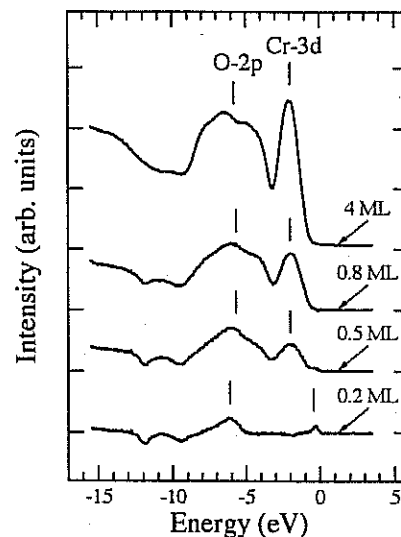FIG. 4. A series of UPS difference spectra generated by subtracting the normalized O_2/Pt(111) spectrum from each CrO_x/Pt(111) spectrum. The three lowest CrO_x coverages correspond to the observance of the $p(2\times2)$ phase and the 4 ML coverage to the $(\sqrt{3}\times\sqrt{3})R30°$ phase.

trace amounts of oxygen are adsorbed on the Pt surface. In addition, two small peaks at ~9 eV and ~12 eV are observed which corresponds to the adsorption of CO during the oxygen dosing.

To better differentiate the CrO_x emission features from the Pt features, a series of difference spectra were generated by subtracting the normalized O_2/Pt(111) spectrum from each CrO_x/Pt(111) spectrum and are shown in Fig. 4. The oxygen dosed Pt spectrum was chosen for the subtraction instead of the clean Pt to account for trace amounts of oxygen which adsorb on the Pt regions of the surface during CrO_x growth. The scale factors for the normalization were determined by calculating the ratio of the height of the emission near the Fermi edge of each CrO_x/Pt(111) spectrum to the height of the O_2/Pt(111) Fermi edge. To check the accuracy of this procedure, difference spectra were also generated using the relative attenuation of the Pt 4f emissions to determine the scale factors, and these spectra showed similar results to those generated using the ratios of the Fermi edges. The three lowest CrO_x coverages in Fig. 4 are within the region where a $p(2\times2)$ overlayer is observed, and the 4 ML spectrum is within the $(\sqrt{3}\times\sqrt{3})R30°$ region and corresponds to a $Cr_2O_3(0001)$ overlayer. From comparison of the 4 ML spectrum with the DOS for Cr_2O_3 in Fig. 2, it can be seen that the Cr 3d band is shifted ~1 eV higher in binding energy than is predicted by the DOS calculations, and the O 2p band is shifted ~1.5 eV to lower binding energy. These shifts are in agreement with previously published UPS results for the $Cr_2O_3(0001)/Cr(110)$ system.[18] There is no apparent shift in the positions of the Cr 3d and O 2p bands of the 0.5 and 0.8 ML coverages with respect to those of the 4 ML overlayer. However, there is a change in the ratio of the heights of the Cr 3d intensity to that of the O 2p intensity: 0.7 for the 0.5 ML coverage, 1.0 for the 0.8 ML coverage, and 1.4 for the 4 ML coverage. The most dramatic

changes in the UPS spectra occur for the 0.2 ML coverage. At this coverage, emission near the Fermi level is observed, the O $2p$ emission is only ~4 eV wide, and the onset of O $2p$ emission is shifted ~2 eV higher in binding energy than for the spectra at higher coverages. Another feature which is observed for the three lowest coverages is two "negative" peaks at ~9 eV and ~12 eV. These peaks arise from CO which has adsorbed on the oxygen dosed Pt(111) surface and is not present on the surface after CrO_x growth at 300 °C.

V. DISCUSSION

The UPS spectrum in Fig. 4 which most closely resembles the DOS of the Cr_3O_4 is from the 0.2 ML CrO_x coverage. An ~0.5 eV wide emission feature is observed just below the Fermi level which indicates that the overlayer is metallic. A remnant of this peak is also observed for the 0.5 ML coverage but is missing at higher coverages. In addition, the onset of emission from the O $2p$ band is shifted ~2 eV to higher binding energy in comparison with the other coverages which agrees with the difference in the calculated onsets for Cr_2O_3 and Cr_3O_4. Although the onset of emission from the O $2p$ band is ~1.5 eV lower in binding energy than what is predicted by the calculated DOS, this same behavior is observed for the 4 ML spectrum when compared to the calculated DOS for Cr_2O_3 which indicates that this is a systematic error of the calculation technique.

The nature of the $p(2\times2)$ phase which is observed beyond ~0.2 ML of CrO_x coverage is somewhat uncertain. One possible explanation is that the calculated ground state electronic structure of Cr_3O_4 incorrectly represents the electronic structure observed via photoemission. A previous spin-resolved photoemission study of polycrystalline CrO_2 films[19] indicates that this is the case for the calculated DOS of CrO_2. Almost 100% spin polarization was observed for the Cr $3d$ emission from their polycrystalline CrO_2 films which agrees with the prediction that the minority spin channel has no DOS below the Fermi level. However, the onset of the Cr $3d$ emission was observed at ~1.5 eV below the Fermi level which contradicts both our and previous DOS calculations[14,15] and experimental resistivity measurements[6,20] which indicate that CrO_2 is metallic. It was proposed that an interatomic exchange interaction may be the source of these discrepancies. If this were the case for Cr_3O_4, it is expected that *both* the Cr $3d$ and O $2p$ emissions should shift to higher binding energy. This is not observed in the UPS spectra; therefore, it is unlikely that such an exchange interaction is significantly influencing the electronic structure.

Another possible explanation for the nature of the $p(2\times2)$ phase is that it corresponds to a γ-$Cr_2O_3(111)$ phase. In analogy to γ-Fe_2O_3, the γ phase of Cr_2O_3 is also a cubic spinel structure with random, missing Cr, point defects. Since the γ phase has the same stoichiometry as the corundum structured Cr_2O_3, it might also have a similar valence structure. Because the crystal structure is an ill-defined defect structure, calculations of the DOS have not been per-

formed to confirm this. Both octahedrally and tetrahedrally coordinated Cr ions are present in this structure which would give rise to the broadening of the Cr $2p$ core emission which has been observed in previously published XPS data for the $p(2\times2)$ phase.[9] Another factor that should be considered is the experimentally determined lattice constant of γ-Cr_2O_3 which is $a_0 = 8.36$ Å.[8] If the $p(2\times2)$ overlayer maintained the same lattice constant as the bulk γ-Cr_2O_3 value, a splitting of the Pt(111) and the $p(2\times2)$ LEED spots would be observed since there is a relatively large 6% lattice mismatch. No splitting was observed which indicates a pseudomorphic growth mode.

The possibility that the $p(2\times2)$ phase corresponds to a reconstructed $Cr_2O_3(0001)$ surface has also been considered. If the $Cr_2O_3(0001)$ surface were to reconstruct in a $(\sqrt{3}\times\sqrt{3})R\,30°$ pattern with respect to a bulk-terminated $Cr_2O_3(0001)$ surface, this would result in a $p(2\times2)$ LEED pattern with respect to the Pt(111) substrate. In fact, a previous study of the $Cr_2O_3(0001)/Cr(110)$ system has revealed that this surface reversibly transforms from a (1×1) symmetry with respect to the $Cr_2O_3(0001)$ surface at room temperature to a $(\sqrt{3}\times\sqrt{3})R\,30°$ overlayer structure at ~150 K which then converts back to a (1×1) symmetry as the temperature is lowered below ~100 K.[21] Since the onset of antiferromagnetic ordering is often accompanied by lattice distortions, they proposed that the transformation from the room temperature (1×1) symmetry to the $(\sqrt{3}\times\sqrt{3})R\,30°$ overlayer structure at lower temperatures might be driven by antiferromagnetic coupling of the surface chromium ions to those in the second layer. It is possible that the magnetic interaction within the initial $p(2\times2)$ bilayer of CrO_x on Pt(111) is significantly different than the interaction for subsequent multilayers which may increase the temperature at which a reconstruction might occur to room temperature. On the other hand, no structural analysis of the $(\sqrt{3}\times\sqrt{3})R\,30°$ $Cr_2O_3(0001)/Cr(110)$ overlayer has been published at this time. Therefore, it is also possible that the $Cr_2O_3(0001)/Cr(110)$ system is undergoing a transformation to the γ-Cr_2O_3 phase at low temperatures instead of a simple surface reconstruction. As mentioned above, a broadening of the Cr $2p$ levels is observed with XPS.[9] For a reconstructed $Cr_2O_3(0001)$, significant broadening is not generally expected since a rearrangement of the surface Cr ions should not have much of an effect on their local chemical environment.

Another point of interest is the apparent lack of new UPS features which would correspond to the mixing of Pt and Cr_2O_3 states for coverages greater than ~0.2 ML. This may be explained by considering the growth morphology of the CrO_x film. The previously mentioned STM analysis of this system shows a step flow growth mode with a 2 ML film height.[9] If there were any changes in the electronic structure and these changes were confined to the interface region, the new features would be buried under the bilayer and may not be easily detected in surface-sensitive UPS spectra. Another consequence of the step flow growth mode is the possibility that the crystal structure of the CrO_x overlayer could be con-

trolled by changing the substrate misorientation. Since the initial formation of Cr_3O_4 may be a direct result of the interaction of the CrO_x with the step edges, it might be possible to grow a uniform Cr_3O_4 overlayer through the first two monolayers of growth by using a vicinal substrate.

VI. CONCLUSIONS

The similarity of the calculated DOS of Cr_3O_4 and the measured UPS spectra for low CrO_x coverages indicates that chromium oxide initially crystallizes in a cubic spinel structure. For coverages higher than ~ 0.2 ML, the measured UPS spectra of the $p(2\times2)$ phase deviate significantly from the calculated DOS of Cr_3O_4. The most probable origin of the $p(2\times2)$ phase is a pseudomorphic γ-$\text{Cr}_2\text{O}_3(111)$ overlayer, but it is also possible that the $p(2\times2)$ phase results from a reconstructed $\text{Cr}_2\text{O}_3(0001)$ film. Ultimately, further structural analysis of the $p(2\times2)$ phase using a technique such as LEED-IV is required before the crystalline structure can be definitely determined.

ACKNOWLEDGMENTS

[1]H. C. Galloway, J. J. Benítez, and M. Salmeron, Surf. Sci. **298**, 127 (1993).
[2]H. C. Galloway, J. J. Benítez, and M. Salmeron, J. Vac. Sci. Technol. A **12**, 2302 (1994).
[3]C. A. Ventrice, Jr., Th. Bertrams, H. Hannemann, A. Brodde, and H. Neddermeyer, Phys. Rev. B **49**, 5773 (1994).
[4]H. Hannemann, C. A. Ventrice, Jr., T. Bertrams, A. Brodde, and H. Neddermayer, Phys. Status Solidi A **146**, 289 (1994).
[5]H. Kuhlenbeck and H.-J. Freund, in *Growth and Properties of Ultrathin Epitaxial Layers*, edited by D. A. King and D. P. Woodruff (Elsevier, New York, 1997), Chap. 9, pp. 340–374.
[6]B. L. Chamberland, CRC Crit. Rev. Solid State Sci. **7**, 1 (1977).
[7]M. Hansen and K. Anderko, *Constitution of Binary Alloys*, 2nd ed. (McGraw-Hill, New York, 1958).
[8]R. W. G. Wyckoff, *Crystal Structures*, 2nd ed. (Interscience, New York, 1969).
[9]L. Zhang, M. Kuhn, and U. Diebold, Surf. Sci. **375**, 1 (1997).
[10]J. A. Rodriguez, S. Chaturvedi, M. Kuhn, J. van Ek, U. Diebold, P. S. Robbert, H. Geisler, and C. A. Ventrice, Jr., J. Chem. Phys. **107**, 9146 (1997).
[11]O. K. Andersen, Phys. Rev. B **12**, 3060 (1975).
[12]W. Kohn and L. J. Sham, Phys. Rev. **140**, A1133 (1965).
[13]U. von Barth and L. Hedin, J. Phys. C **5**, 1629 (1972).
[14]H. van Leuken and R. A. de Groot, Phys. Rev. B **51**, 7176 (1995).
[15]K. Schwarz, J. Phys. F **16**, L211 (1986).
[16]D. S. McClure, J. Chem. Phys. **38**, 2289 (1963).
[17]B. B. Krichevtsov, V. V. Pavlov, R. V. Pisarev, and V. N. Gridnev, Phys. Rev. Lett. **76**, 4628 (1996).
[18]C. A. Ventrice, Jr., D. Ehrlich, E. L. Garfunkel, B. Dillmann, D. Heskett, and H.-J. Freund, Phys. Rev. B **46**, 12892 (1992).
[19]K. P. Kämper, W. Schmitt, T. Güntherodt, R. J. Gambino, and R. Ruf, Phys. Rev. Lett. **59**, 2788 (1987).
[20]D. S. Rodbell, J. M. Lommel, and R. C. DeVries, J. Phys. Soc. Jpn. **21**, 2430 (1966).
[21]M. Bender, D. Ehrlich, I. N. Yakovkin, F. Rohr, M. Bäumer, H. Kuhlenbeck, H.-J. Freund, and V. Staemmler, J. Phys.: Condens. Matter **7**, 5289 (1995).